Journal of the Ceramic Society of Japan 124 [9] 911-914 2016 Full paper

Reactive sintering and piezoelectric properties of $0.94Bi_{0.5}Na_{0.5}TiO_3$–$0.06BaTiO_3$ ceramics with ZnO additive

Tasuku KAWASHIMA* **and Yoshikazu SUZUKI*,**,†**

***Graduate School of Pure and Applied Sciences, University of Tsukuba, 1–1–1 Tennodai, Ibaraki 305–8573, Japan**
****Faculty of Pure and Applied Sciences, University of Tsukuba, 1–1–1 Tennodai, Ibaraki 305–8573, Japan**

Bismuth sodium titanate ($Bi_{0.5}Na_{0.5}TiO_3$, BNT) and its solid-solution with $BaTiO_3$ (BNT–BT) are promising lead-free piezoelectric ceramics. Around the morphotropic phase boundary (MPB), the 0.94BNT–0.06BT composition shows high piezoelectric performance. In this paper, we have investigated the effect of ZnO-doping on the reactive sintering and piezoelectric properties of 0.94BNT–0.06BT ceramics. Bi_2O_3, anhydrous Na_2CO_3, TiO_2 (anatase), $BaCO_3$ and ZnO powders were wet ball-milled in ethanol, cold isostatically pressed at 200 MPa for 10 min, and reactively sintered at 1150°C for 2 h in air. The relative density drastically increased from 83.3% (without ZnO) to 93.7% (with 0.5 mol% ZnO). The sample with 0.5 mol% ZnO showed the highest piezoelectric constant d_{33} of 124 pC/N. Even by the one-step reactive sintering, the d_{33} value was comparable with that of the two-step conventional sintering.

Key-words : Bismuth sodium titanate, Barium titanate, Morphotropic phase boundary, Reactive sintering, Piezoelectric property

[Received March 4, 2016; Accepted July 4, 2016]

1. Introduction

Currently, lead-based piezoelectric ceramics [e.g. $Pb(Zr,Ti)O_3$ or PZT families] are widely used, however, many problems are suggested during the manufacturing and after the use because of the toxicity of lead. Among the many studies about lead-free piezoelectric ceramics, bismuth sodium titanate ($Bi_{0.5}Na_{0.5}TiO_3$, BNT) is promising due to its high Curie temperature of 320°C,[1),2)] relatively high piezoelectric constant of $d_{33} = 72.9$ pC/N,[3)] facile processing, and so on. Takenaka et al.[4)] reported that much higher piezoelectricity was obtained for $Bi_{0.5}Na_{0.5}TiO_3$–$BaTiO_3$ (BNT–BT) solid solutions; there is a morphotropic phase boundary (MPB) around the 0.94BNT–0.06BT composition, which showed the maximum piezoelectricity ($d_{33} = 125$ pC/N).

Recently, we have reported an environmental friendly processing of $BaTiO_3$ piezoelectric ceramics, viz., one-step reactive sintering.[5)] Besides the low energy consumption, the merits of reactive sintering are to reduce the contamination during the milling after calcination and to suppress the compositional change by volatilization. However, the reactive sintering method is hardly applied for the industrial process for piezoelectric ceramics because of its less densification compared with the conventional sintering (i.e., two-step heating including preliminary calcination and main sintering). The relative density of the reactively sintered $BaTiO_3$ (without additive) was at most ~85%.[5)]

To improve the densification of BNT–BT ceramics, oxide sintering additives were used not only for the conventional sintering (e.g. with Nb_2O_5, La_2O_3, Co_2O_3 and CeO_2[6),7)]) but also for the reactive sintering (with In_2O_3[8)]). Zhou et al.[8)] reported that In_2O_3-doping was effective to improve the densification, and the 0.93BNT–0.07BT ceramics with 0.16 wt.% In_2O_3 doping, reactively sintered at 1150°C for 3 h, exhibited a high piezoelectric constant of $d_{33} = 205$ pC/N. However, the relative density, the elemental distribution and the temperature dependence of dielectric constants were not reported in their report.

In this paper, we have tried to use another oxide additive, ZnO, for the reactive sintering of 0.94BNT–0.06BT ceramics. ZnO was used as an additive for the conventional sintering of BT[9)] and BNT ceramics,[10),11)] however as far as we know, it is not used for the reactive sintering of BNT–BT. The effect of ZnO doping on the density, piezoelectric properties and the temperature dependence of dielectric constants were investigated in detail.

2. Experimental procedure

Targeting the final compositions of $0.94BNT–0.06BT + 0.01xZnO$ ($x = 0$–5), Bi_2O_3 (99.9% purity, Wako Pure Chemical Industries Ltd., Osaka, Japan), anhydrous Na_2CO_3 (99.8% purity, Wako), TiO_2 (anatase) (99% purity, Kojundo Chemical Laboratory Co. Ltd., Saitama, Japan), $BaCO_3$ (99.9% purity, Wako) and ZnO (99.9% purity, Wako) powders were used. These powders were wet ball-milled in ethanol with ZrO_2 balls for 8 h in a polystyrene bottle. The slurry was dried in a rotary evaporator to obtain the mixed powders, and then, they were sieved through a 150 mesh (<100 μm) screen. Green disk-shape pellets (15 mm in diameter and ~2 mm in thickness) was prepared by uniaxial metallic die pressing (22.2 MPa) for 1 min. The green compacts were cold isostatically pressed at 200 MPa for 10 min. The green samples were degassed at 500°C for 2 h, and then sintered at 1150°C for 2 h in an air atmosphere, with heating late of 100°C/h in each step. In an alumina crucible, platinum wires were used to prevent the direct contact between the samples and the crucible.

Constituent phases of sintered samples were analyzed by X-ray diffraction (XRD, Multiflex, Cu-K_α, 40 kV and 40 mA, Rigaku, Japan). Prior to the XRD measurement, sintered samples were crushed and pestled with an agate mortar using ethanol, and the XRD patterns were collected in the range of $2\theta = 10$–70°. ICDD-JCPDS database was used to identify the constitution phases.

Surface microstructure of the sintered samples was observed by scanning electron microscopy (SEM, JSM-5600/SV, JEOL,

† Corresponding author: Y. Suzuki; E-mail: suzuki@ims.tsukuba.ac.jp

DOI http://dx.doi.org/10.2109/jcersj2.16051

Japan); the samples were coated with Pt by sputtering before the observation. The elemental distribution of the sample was analyzed by energy dispersive X-ray spectroscopy (EDS, Oxford SwiftED3000, equipped with a TM3000 Table Microscope, Hitachi, Japan). For the EDS analysis, the sample was mirror polished with 9, 3 and 0.5 µm diamond slurries.

After gentle grinding, sintered samples were polished into 1.2 mm in thickness with waterproof abrasive papers (#800). After polishing, the density of disk samples was calculated from dimensions and mass. Silver paste was coated on the both sides of polished samples and sintered at 550°C for 30 min in air to form Ag electrodes. Samples for the piezoelectric measurements were poled at 80°C for 10 min in silicone oil bath with applying 4 kV/mm of electric field. After 1 day, the piezoelectric constant d_{33} was measured with d_{33} meter (ZJ-6B, Institute of Acoustics Chinese Academy of Sciences, China). Before and after the poling of disk samples, temperature dependency of dielectric constants was measured by impedance analyzer (Agilent HP4192A, Santa Clara, CA, USA) at 1 kHz. After the poling of samples, the planar electromechanical coupling factor (k_p) and mechanical quality factor (Q_m) were measured by the resonance-antiresonance method by using the impedance analyzer. For the calculation of k_p and Q_m, the following equations were used:

$$k_p = \frac{1}{\sqrt{0.395 * \frac{f_r}{f_a - f_r} + 0.574}}$$

$$Q_m = \frac{1}{2\pi f_r R_1 C_f \left\{1 - \left(\frac{f_r}{f_a}\right)^2\right\}}$$

where f_r (Hz): Resonance frequency, f_a (Hz): Antiresonance frequency, R_1 (Ω): Impedance at f_r, and C_f (F): Capacity at 1 kHz.

3. Results and discussion

Figure 1 shows XRD patterns of sintered samples. Almost single phase of the rhombohedral perovskite structure was obtained for each sample. The peaks were slightly shifted to lower angles with increasing x [Fig. 1(b)], which can be attributed to the lattice expansion by the substitution of Zn^{2+} [0.740 Å (6-coordination)] for Ti^{4+} [0.605 Å (6-coordination)].[12] Only in $x = 5$, a very small peak was detected around $2\theta = 35°$, which can be attributed to an impurity phase, most probably Zn_2TiO_4 (inverse spinel structure). The strongest peak of Zn_2TiO_4 locates at $2\theta = 35.1°$.

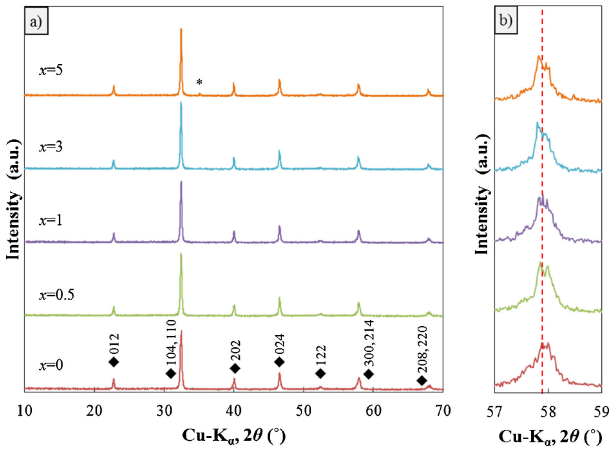

Fig. 1. XRD patterns of sintered 0.94BNT–0.06BT + 0.01xZnO (x = 0–5) sintered at 1150°C for 2 h: (a) 2θ = 10–70° and (b) 2θ = 57–59°.

Figure 2 demonstrates the surface microstructure of sintered samples. Comparing Figs. 2(a) and 2(b) ($x = 0$ and 0.5), the grain shape at the surface was changed from roundish to cubic-like, and the grain size increased with increasing ZnO doping. The samples with ZnO doping had dense microstructure, and that of $x = 0.5$ showed the finest microstructure among them. With increasing ZnO content [Figs. 2 (c)–2(e)], cubic-like grain shape gradually changed into irregular shapes. In Figs. 2(d)–2(e) ($x = 3$ and 5), grain boundary glassy phase was observed, which contained somewhat more Na^+ ions (confirmed by EDS analysis, see Fig. S1). In Fig. 2(e) ($x = 5$), some second-phase particles with triangle shape were observed; the second phase will be Zn_2TiO_4, which is in good agreement with the XRD analysis. **Figure 3** shows the EDS analysis for the mirror polished sample of $x = 5$. Within the sample (i.e., not on the surface) [Fig. 3(a)], the darker contrast corresponds to the glassy phase (Na, Ti, and Zn rich), and the brighter contrast corresponds to the matrix. Bi was mainly dispersed in the matrix, whereas Ba and Ti were dispersed in both areas.

Figure 4 shows the density changes with ZnO doping. The relative density in the figure was calculated from theoritical X-ray density (determined by Rietveld analysis, see Table S1). Note that the theoretical densities of BNT and BT are 5.992[13] and 6.012 g/cm^3,[14] respectively (the glassy phase was ignored in this calculation). The relative density drastically increased from 83.3% ($x = 0$) to 93.6% ($x = 0.5$), and was saturated (ca. 92–95%), which was in good agreement with the SEM observation in Fig. 2. The real relative density (considering the glassy phase and Zn_2TiO_4) will be somewhat higher. According to these results, a small amount of ZnO is effective for the densification. With ZnO doping, the densification was accelerated by the liquid phase formation and the oxygen defect formation (accompanied by the Zn^{2+} substitution into the B-site of the perovskite structure).

Figure 5 shows the temperature dependence of dielectric constant and dielectric loss ($\tan\delta$) at 1 kHz: (a, c) before poling, and (b, d) after poling. In Fig. 5(a), before poling, the peak-top values of dielectric constant were clearly observed for $x = 0$ and 0.5 at ~220°C. However, for $x \geq 1$, the peaks became gentle and the

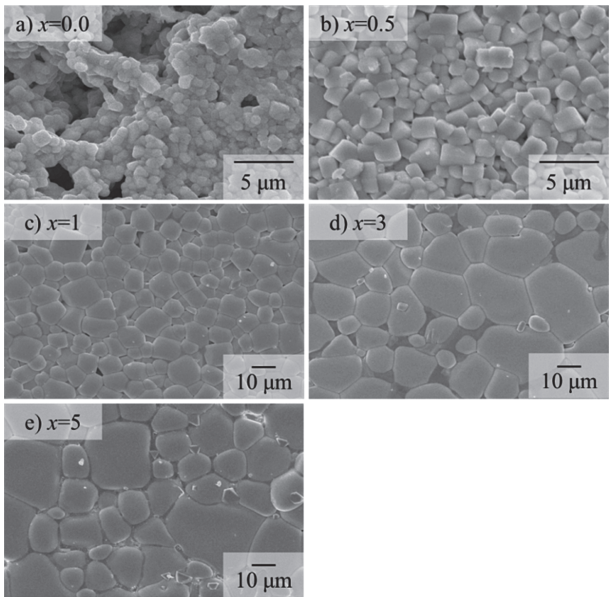

Fig. 2. Surface structure of 0.94BNT–0.06BT + 0.01xZnO (x = 0–5) sintered at 1150°C for 2 h.

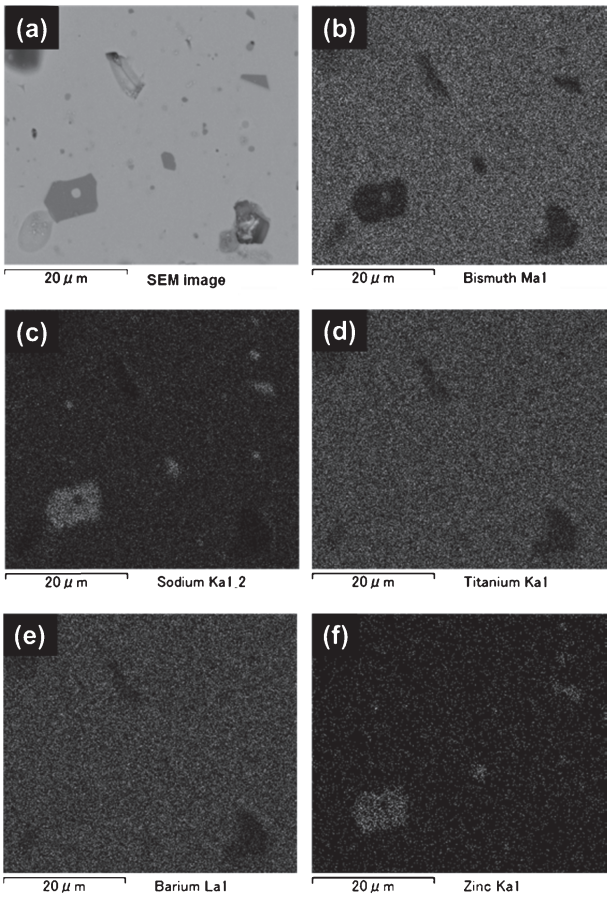

Fig. 3. EDS analysis of 0.94BNT–0.06BT + 0.05ZnO sintered at 1150°C for 2 h: (a) SEM image, (b) Bi, (c) Na, (d) Ti, (e) Ba and (f) Zn. The brightness of Zn was amplified. Before the analysis, the sample was heated at 400–500°C for 30 min to remove the possible contamination from the diamond slurry.

peak-top shifted to somewhat higher temperatures (~230°C). In Fig. 5(b), after poling, clear inflection points were observed at ~100–150°C, which can be attributed to the depoling temperature. The depoling temperature increased with increasing ZnO doping. In Fig. 5(c), before poling, $\tan\delta$ steeply increased for $x \geq 1$, however, $\tan\delta$ kept small for $x = 0$ and 0.5. In Fig. 5(d), after poling, clear inflection points were also observed for $\tan\delta$ ($x = 0.5$), similarly to the dielectric constant.

In Figs. 5(a)–5(d), different trends were seen in each graph shape before and after the $x = 0.5$. The different trends can be explained as follows. Thinking about the effective ionic radius, doped Zn^{2+} ions tend to substitute the Ti^{4+} ions in the B-site, and hence, oxygen defects will be introduced to compensate the charge balance. Such oxygen defects can act as conductive paths, which resulted in the increase of the electric conductivity. Moreover, at >200°C, the charge distributes not only at the surface but also the sample inside, which increases the dielectric constants and $\tan\delta$.

After the poling, the planar electromechanical coupling factor (k_p) and mechanical quality factor (Q_m) were calculated from the

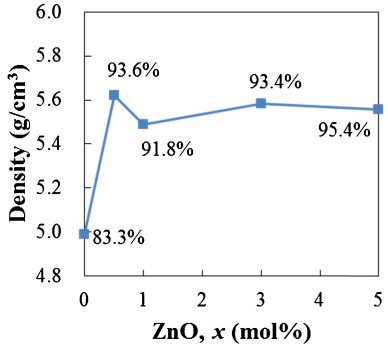

Fig. 4. Density of 0.94BNT–0.06BT + 0.01xZnO (x = 0–5) sintered at 1150°C for 2 h.

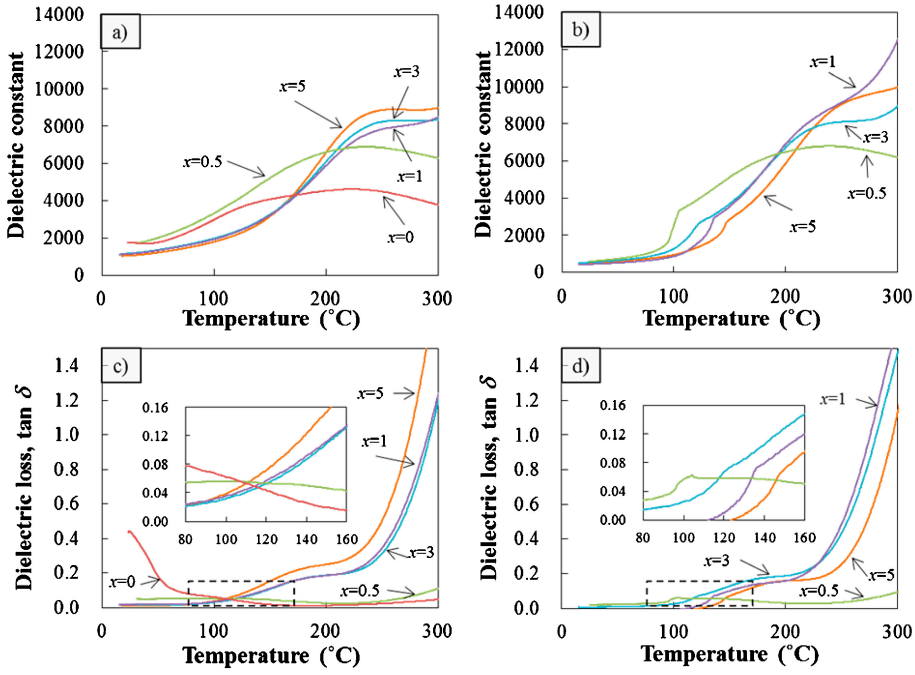

Fig. 5. Temperature dependence of dielectric constant and dielectric loss at 1 kHz; (a, c) before poling, and (b, d) after poling. In (b, d), the result of $x = 0$ after poling was not shown because the $x = 0$ sample was so porous that the high electric field could not be applied.

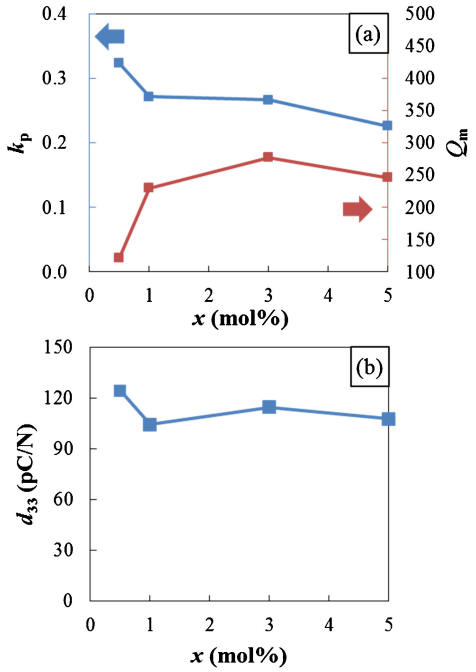

Fig. 6. Piezoelectric properties of 0.94BNT–0.06BT + 0.01xZnO (x = 0.5–5) sintered at 1150°C for 2 h; (a) k_p and Q_m, (b) d_{33}. The result of $x = 0$ was not shown because the $x = 0$ sample was so porous that the high electric field could not be applied.

frequency dependence of impedance for each sample [**Fig. 6**(a)]. The highest k_p was observed on $x = 0.5$, which suggests the highest piezoelectric constant is expected on this composition. Q_m increased with increasing ZnO doping. High Q_m materials tend to have higher Curie temperature and lower piezoelectric constant than low Q_m materials, which are in good accordance with Fig. 5(b).

Figure 6(b) represents the piezoelectric property. The sample of $x = 0.5$ showed the highest d_{33} value of 124 pC/N. The highest piezoelectric property is attributable to the faceted cubic-like grains and fine microstructure, as can be seen in Fig. 2(b), enabling the easy poling. Somewhat lower d_{33} values for $x \geq 1$ can be explained by the grain growth (>10 µm), as shown in Figs. 2(c)–2(e), and hence, by the lower dielectric constant at room temperature [Fig. 5(a)]. For the $x \geq 1$, d_{33} was almost constant of ~110 pC/N. As discussed in Fig. 3, excess Zn^{2+} ions tend to form the glassy phase, and hence, the BNT–BT matrix composition will be almost constant around the solid solubility limit. Resonance–antiresonance measurements suggest that the further optimization of poling state is still needed in this system (Fig. S2).

From this study, ZnO doping is really effective to obtain dense reactively-sintered BNT–BT; the sample of $x = 0.5$ is favorable for the near-room temperature applications with high piezoelectric properties, and the samples of $x \geq 1$ are suitable for applications at somewhat higher temperatures with moderate piezoelectric properties.

4. Conclusions

In this study, the effect of ZnO doping on the density, piezoelectric properties and the temperature dependence of dielectric constants were investigated.

(1) We succeeded in the densification of reactively sintered 0.94BNT–0.06BT solid solution by doping 0.5 mol% ZnO. The nominal relative density drastically increased from 83.3% (without ZnO) to 93.7% (with 0.5 mol% ZnO).
(2) For all compositions, the depoling temperature was at ~100–150°C.
(3) The sample with 0.5 mol% ZnO showed the highest k_p, the lowest Q_m and the highest d_{33} of 124 pC/N. The sample with 0.5 mol% ZnO is favorable for the near-room temperature applications with high piezoelectric properties, and the samples with ≥1 mol% ZnO are suitable for applications at somewhat higher temperatures with moderate piezoelectric properties.
(4) Even by the one-step reactive sintering, the d_{33} value was comparable with that of the two-step conventional sintering. This result will contribute environmental-friendly processing of lead-free piezoelectric ceramics.

Acknowledgement We thank Prof. Tamotsu Koyano at Cryogenics Division, Research Facility Center, University of Tsukuba for his help on SEM observation. We also thank Dr. Tohru S. Suzuki at NIMS for his kind help on EDS analysis.

References

1) P. K. Panda, *J. Mater. Sci.*, 44, 5049–5062 (2009).
2) R. Zuo, S. Su, Y. Wu, J. Fu, M. Wang and L. Li, *Metter. Chem. Phys.*, 110, 311–315 (2008).
3) Y. Hiruma, H. Nagata and T. Takenaka, *J. Appl. Phys.*, 105, 084112 (2009).
4) T. Takenaka, K. Maruyama and K. Sakata, *Jpn. J. Appl. Phys.*, 30, 2236–2239 (1991).
5) T. Kawashima and Y. Suzuki, *J. Ceram. Soc. Japan*, 123, 83–85 (2015).
6) H.-D. Li, C.-D. Feng and W.-L. Yao, *Mater. Lett.*, 58, 1194–1198 (2004).
7) S. Wu, Q. Xu, X. Zhao, T. Liu and Y. Li, *Mater. Res. Bull.*, 41, 1345–1352 (2006).
8) T.-S. Zhou, R.-X. Huang, X.-Z. Shang, F. Peng, J.-Y. Guo, L.-Y. Chai, H.-S. Gu and Y.-B. He, *Appl. Phys. Lett.*, 90, 182903 (2007).
9) A. C. Caballero, J. F. Fernández, C. Moure, P. Duran and Y. Chiang, *J. Am. Ceram. Soc.*, 81, 939–944 (1998).
10) H. Zhang, S.-J. Fu, W.-J. Long and D.-J. Guo, *Ceram. Int.*, 38, 3237–3242 (2012).
11) Y.-C. Lee, T.-K. Lee and J.-H. Jan, *J. Eur. Ceram. Soc.*, 31, 3145–3152 (2011).
12) R. D. Shannon, *Acta Crystallogr., Sect. A:*, 32, 751–767 (1976).
13) G. O. Jones and P. A. Thomas, *Acta Crystallogr., Sect. B:*, 58, 168–178 (2002).
14) H. E. Swanson, R. K. Fuyat and G. M. Ugrinic, *Standard X-ray Diffraction Powder Patterns*, 3, 45–46 (1954).